Electronic Supplementary Information for

Polysulfide Rejection Layer from Alpha-Lipoic Acid for High Performance Lithium–Sulfur Battery

Jongchan Song[a], Hyungjun Noh[a], Hongkyung Lee[a], Je-Nam Lee[a], Dong Jin Lee[a], Yunju Lee[b], Chul Hwan Kim[c], Yong Min Lee[b,*], Jung-Ki Park[a,*] and Hee-Tak Kim[a,*]

[a] *Department of Chemical and Biomolecular Engineering, Korea Advanced Institute of Science and Technology (KAIST), 373-1, Guseong-dong, Yuseong-gu, Daejeon 305-701, Republic of Korea*

[b] *Department of Chemical and Biological Engineering, Hanbat National University, Deokmyoung-dong, Yuseong-gu, Daejeon 305-719, Republic of Korea*

[c] *Orange Power Ltd., #102, 187 Techno2-ro, Yuseong-gu, Daejeon 305-500, Republic of Korea*

* Corresponding author. Tel.: +82-42-350-3965; E-mail addresses: jungpark@kaist.ac.kr

** Co-corresponding author 1. Tel.: +82-42-350-3916; heetak.kim@kaist.ac.kr

** Co-corresponding author 2. Tel.: +82-42-821-1549; yongmin.lee@hanbat.ac.kr

Supporting Figures

S1. Cyclic voltammetry analysis of the Li-S cells with the ALA-containing electrolyte

S2. Characterization of the poly(ALA) layer

S3. Polysulfide rejection by the poly(ALA) layer

S4. Electrochemical analysis of the Li-S cell with the ALA-containing electrolyte

S5. Donnan exclusion by the poly(ALA) layer

S6. Li ion conduction through the poly(ALA) layer

S1. Cyclovoltammetic analysis of the Li-S cells with the ALA-containing electrolyte

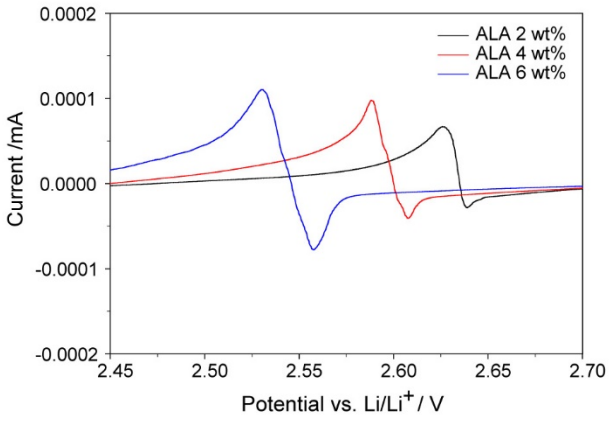

Fig. S1.1. Narrowed potential region from the initial cathodic scan in the CV plots for the Li–S cells with various concentrations of the ALA-containing electrolyte at a scan rate of 0.05 mV s^{-1}.

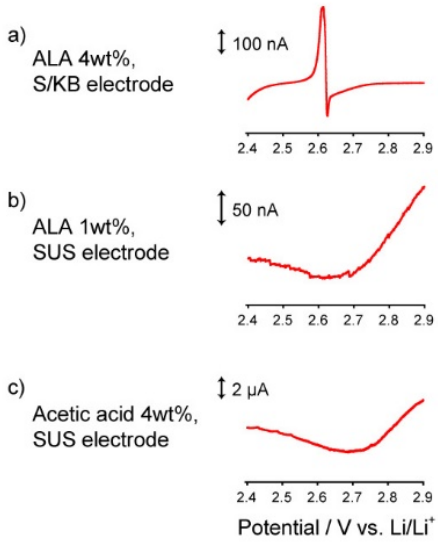

Fig. S1.2. Narrowed potential region from the initial cathodic scan in the CV plots for the cells consisted of Li metal as a counter electrode and various type of working electrodes; a) S/KB electrode, b) SUS electrode, and c) Li/SUS cell with 4wt% acetic acid-containing electrolyte.

Potential scan rate is fixed to 0.05 mV s^{-1}.

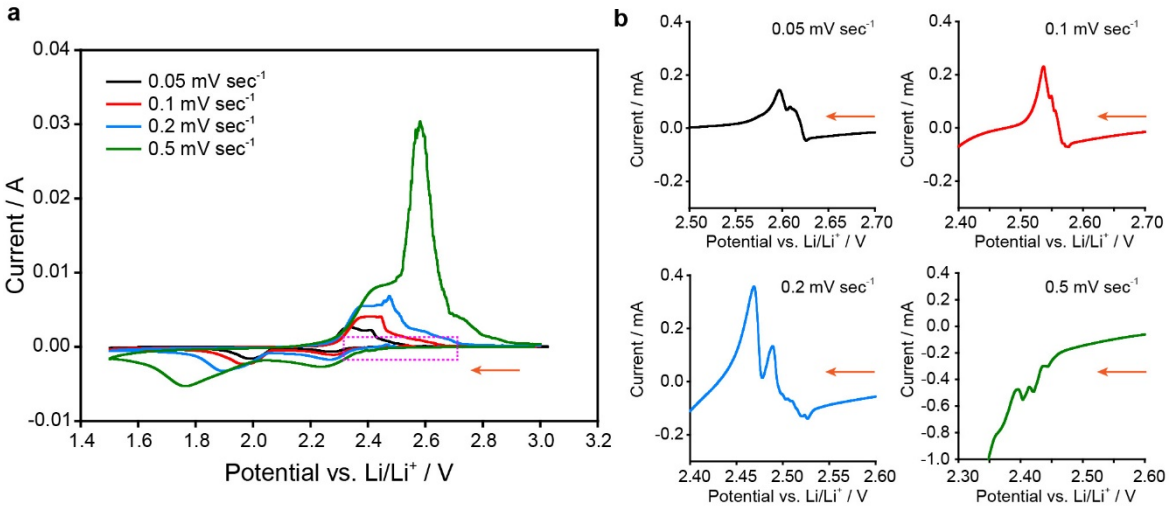

Fig. S1.3. CV plots for the Li-S cells with 4wt% ALA in the electrolyte at various scan rates and (b) magnified cyclic voltammetry curves (dashed box in Fig. a) in the potential range of 2.3–2.7 V.

The CV plots at different scan rates of 0.05, 0.1, 0.2, and 0.5 mV s^{-1} were compared in Fig. S1.3. The first cathodic peak assigned as the 'electrochemical' reduction of acidic protons at around 2.4–2.6 V becomes larger with increasing scan rate. However, subsequent 'electrochemical' anodic peak was increased with increasing scan rate up to 0.2 mV s^{-1}. At the higher scan rates (≥ 0.5 mV s^{-1}), the oxidation peaks were not evident, which strongly indicates the reactions have ECE mechanism.

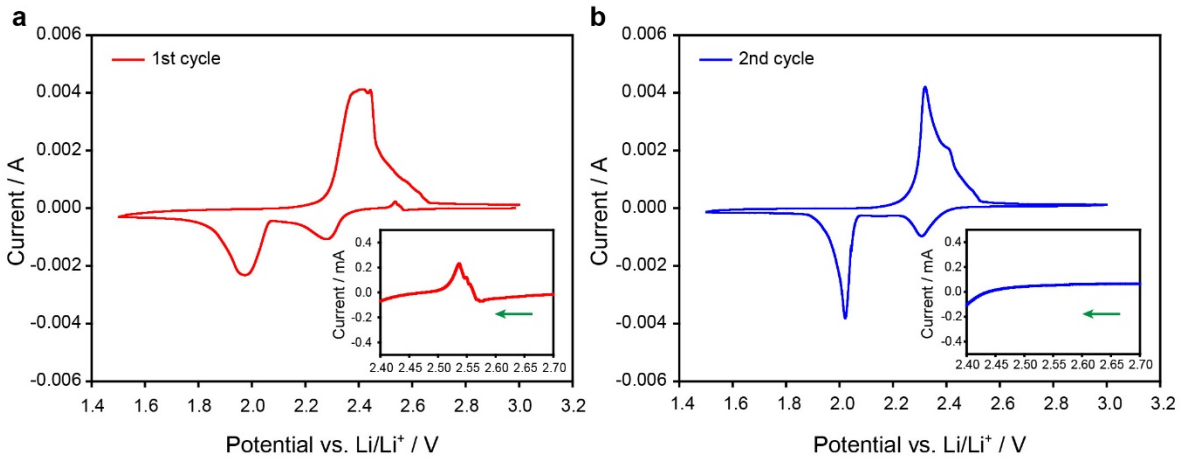

Fig. S1.4. Cyclic voltammetry curves for the Li–S cells with 4 wt% ALA in the electrolyte at (a) the 1st and (b) 2nd cycle (Scan rate: 0.1 mV s^{-1}, the arrows indicate scan direction.).

S2. Characterization of the poly(ALA) layer

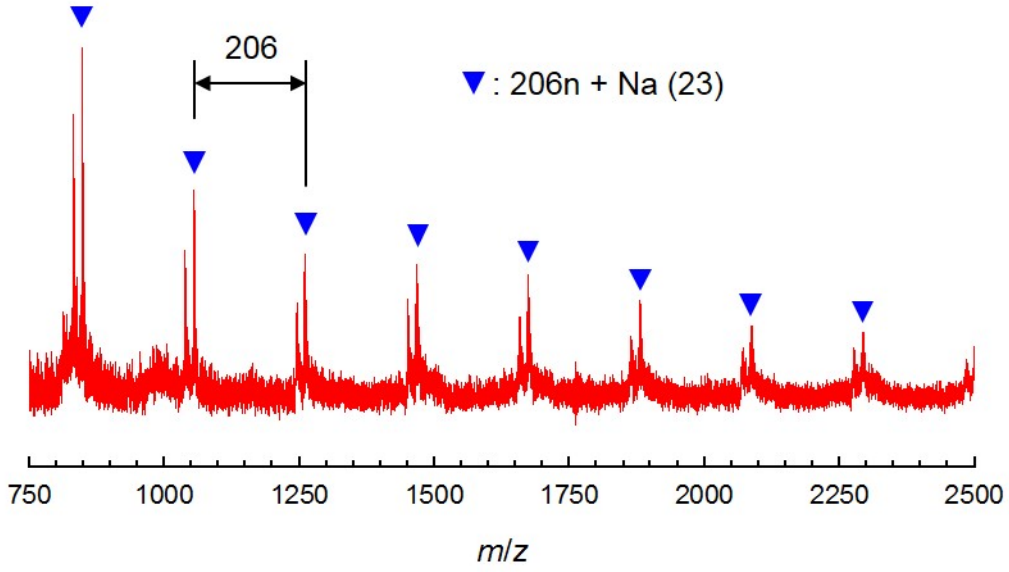

Fig. S2.1. MALDI-TOF mass spectrum of the poly(ALA) layer formed on the SUS electrode during the cathodic scan.

m/z	Intensity (N_i)	$N_i m_i$ ($\times 10^5$)	$N_i m_i^2$ ($\times 10^9$)
847.2	1597.5	13.536	1.1469
1053.4	950.0	10.008	1.0542
1261.5	652.5	8.231	1.0384
1467.5	618.0	9.069	1.3309
1673.6	573.0	9.590	1.6049
1879.6	447.5	8.411	1.5810
2088.6	300.0	6.266	1.3087
2293.7	308.0	7.065	1.6205

The number-average molecular weight (M_n) and weight-average molecular weight (M_w) of the polyALA was determined by MALDI-TOF mass spectrometry using the following equations.

$$M_n = \frac{\sum N_i m_i}{\sum N_i}, \qquad M_w = \frac{\sum N_i m_i^2}{\sum N_i m_i} \qquad (1)$$

N_i and m_i represent the number of moles of each polymer species and the molar mass of that species, respectively. The mass spectrum of the poly(ALA) in the presence of NaI as a cationic reagent and 2,5-dihydroxybenzoic acid (DHBA) as a matrix showed a series of ions repeating at an interval of 206 g mol^{-1} in the range 750–5,000 $[206n + Na(23)]^+$. From equation (1), the M_n and M_w of poly(ALA) were calculated as 1,325 and 1,480, respectively. The degree of polymerization was 6.42, based on the molecular weight of the ALA monomer (206.33 g mol^{-1}).

S3. Polysulfide rejection by the poly(ALA) layer

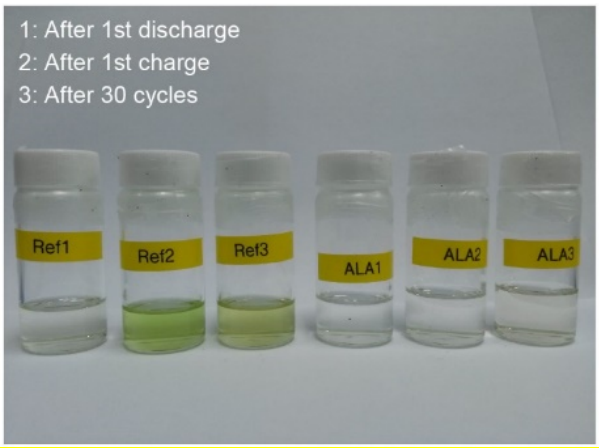

Fig. S3.1. Digital photographic images of the electrolytes with and without 4 wt% ALA (1) after 1st discharge, (2) after 1st charge, and (3) after 30 cycles.

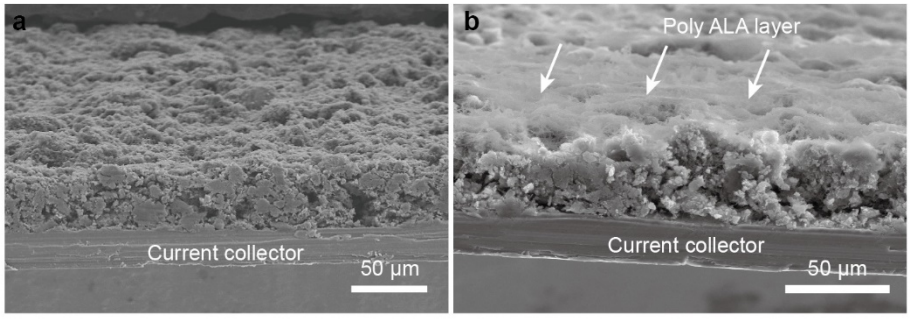

Fig. S3.2. Typical SEM images of cross-sections of the sulfur electrode for (a) the reference cell and (b) the cell with 4 wt% ALA-containing electrolyte.

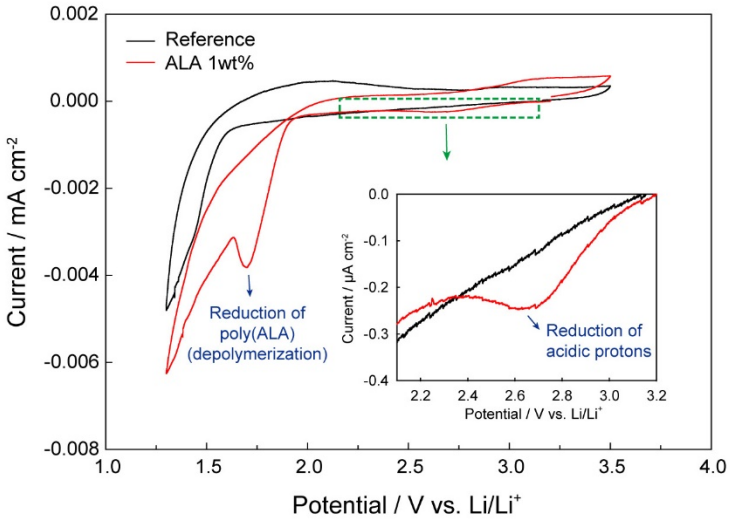

Fig. S3.3. Cyclic voltammetry curves for the Li/SUS cells with 1 wt% and without ALA in the electrolyte at a fixed scan rate of 0.05 mV s^{-1}. CV plots with magnified potential range are shown in inset of the figure.

S4. Electrochemical analysis of the Li-S cell with the ALA-containing electrolyte

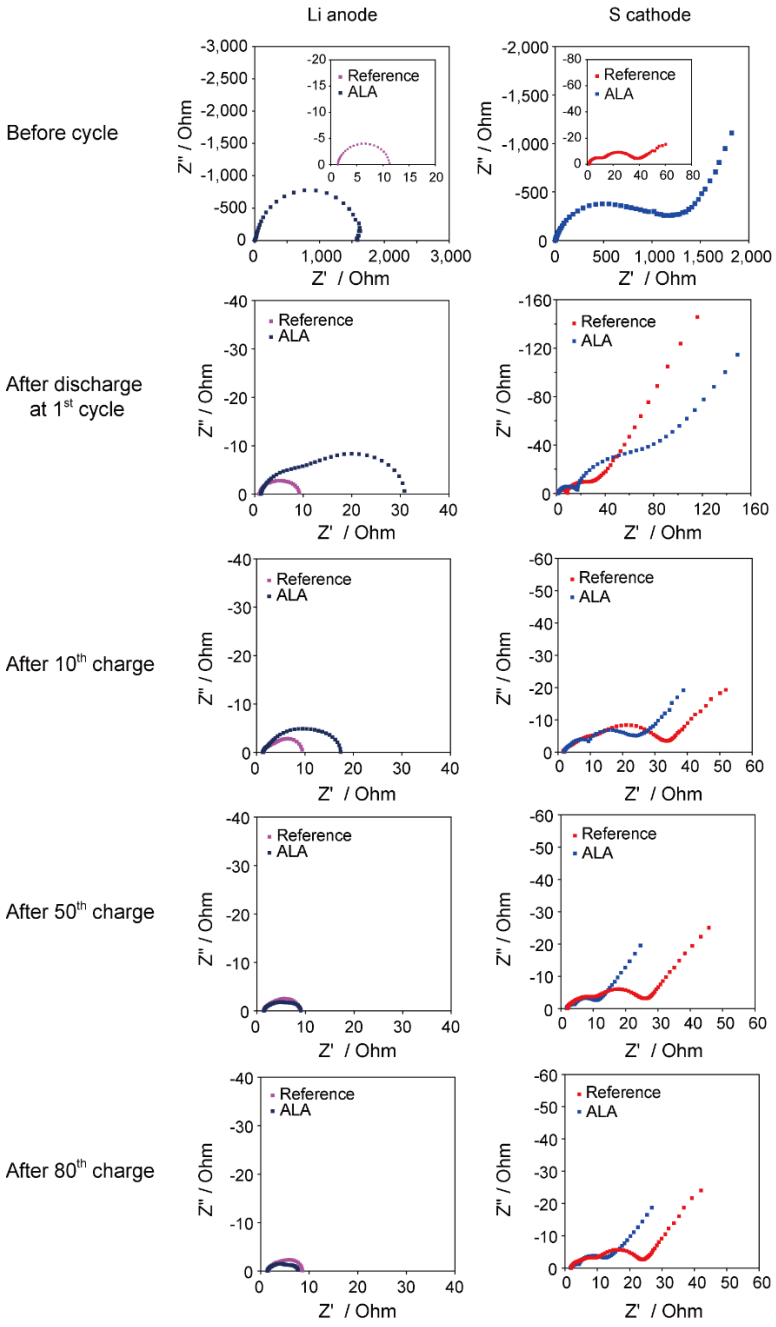

Fig. S4.1. Nyquist impedance plots for the Li anode and sulfur cathode in a three-electrode cell configuration at various cycles for the reference cell and the cell with 4 wt% ALA-containing electrolyte.

The influence of the poly(ALA) layer on the electrochemical process of the sulfur cathode was investigated by electrochemical impedance spectroscopy (EIS) of the Li–S cells in the three-electrode configuration The Nyquist plots of the sulfur cathode impedance before cycling, at the end of the 1st discharge, and after the 10th, 50th, and 80th charges are compared for the reference and the 4 wt% ALA-containing cells in Fig. S4.1. The cathode impedance is characterized by two compressed semi-circles followed by a sloping line. The high frequency semicircle, middle frequency semicircle, and low frequency line may be attributed to ion conduction through the cathode surface film, the charge transfer process at the conducting surface, and ion diffusion through the cathode,[1–4] respectively. The two superimposed semi-circles in the anode impedance spectra can be assigned as contributions from the solid electrolyte interphase (SEI) layer (higher frequencies) and charge transfer reaction (lower frequencies).

Before cycling, the ALA cell revealed abnormally large semi-circles in both the cathode and anode impedance spectra (Fig. S4.1). These were attributed to the strong adsorption of ALA monomers, as reported for carbon and gold electrodes, whereupon ALA forms self-assembled monolayers (SAMs) and hinders both ionic conduction and charge transfer reactions at the electrode interface. To confirm ALA adsorption on the electrode surface, a cell with an ALA-adsorbed cathode and the reference electrolyte was constructed and the impedance of the cell was compared with the reference cell. The sulfur cathode was immersed in a 2 wt% ALA-containing electrolyte for 12 h and washed with DME several times before cell assembly. As shown in Fig. S4.2, the semi-circles for the ALA-adsorbed cathode were more than 4 times larger than those for the untreated cathode. This clearly demonstrates that the large cathode impedance after cell assembly is attributable to the adsorption of ALA on the sulfur cathode.

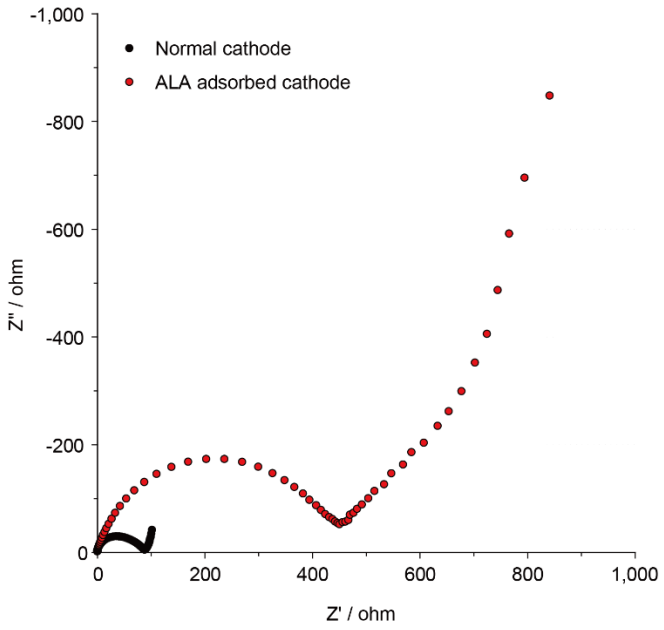

Fig. S4.2. Nyquist plots of the cathode impedance for the ALA-adsorbed sulfur cathode and the reference cathode obtained prior to the first discharge.

The electrochemical removal of the adsorbed ALA on the cathode and anode surface is reflected in the cathode and anode impedances of the ALA-containing cell with longer cycles. The sizes of the high and middle frequency semicircles were greatly reduced after the first discharge for both the cathode and anode as shown in Fig. S4.1, which implies the electrochemical removal of the adsorbed ALA from the two electrodes. Further cycling gradually reduces the film and charge transfer resistance in the ALA-containing cell (Fig. S4.1); the cathode resistance of the ALA-containing cell was smaller than that of the reference after the 10th cycle and the Li anode resistance was also smaller for the ALA-containing cell after the 50th cycle.

With the effect of the adsorbed ALA excluded, the benefit of the poly(ALA) layer on the electrochemical reaction becomes evident. For the reference cell, the cathode impedance is larger than the anode impedance after the initial cycle, which indicates that the cathode performance

dominates the performance of the Li–S battery. The Nyquist plots of the cathode impedance at the 10^{th}, 50^{th}, and 80^{th} cycles clearly show that the *in situ*-formed poly(ALA) layer lowers both the film and charge transfer resistance. This can be explained by the prevention of Li_xSO_y formation as indicated by the XPS analysis (Fig. 3). According to the following equation for Li_xSO_y formation, the negatively charged solvent degradation products react with the PS anion.

$$-O^-Li^+ + S_n^{2-} - e^- \rightarrow Li_xSO_y + S_{n-1}^{2-}$$

The poly(ALA) layer can reject the negatively charged solvent degradation products as it does the negatively charged PS. Therefore, side reaction can also be mitigated with the poly(ALA) layer.

S5. Donnan exclusion by the poly(ALA) layer

Let us consider the electrolyte-swollen poly(ALA) layer with a carboxylate concentration of $\overline{C}_{COO^-}$ in a solution of Li_2S_n and LiTFSI. C_{Li^+}, C_{TFSI^-}, and $C_{S_n^{2-}}$ are the concentrations of Li^+, $TFSI^-$, and S_n^{2-} in the cathode electrolyte phase, respectively. For the electrolyte-swollen poly(ALA) layer, the concentrations of Li^+, $TFSI^-$, and S_n^{2-} are denoted as $\overline{C}_{Li^+}$, $\overline{C}_{TFSI^-}$, and $\overline{C}_{S_n^{2-}}$, respectively.

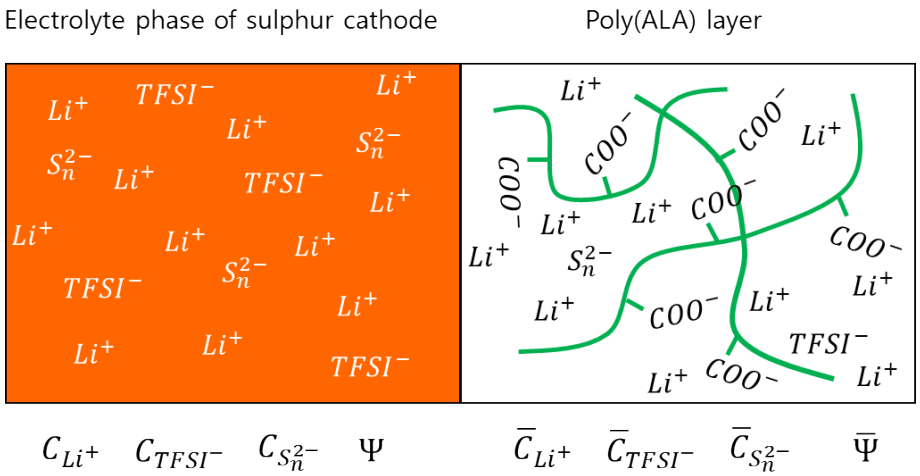

Fig. S5.1. Schematic illustration of the cathode electrolyte phase and the electrolyte-swollen poly(ALA) layer in equilibrium.

From electroneutrality considerations, for the electrolyte phase in the sulfur cathode,

$$C_{Li^+} = C_{TFSI^-} + 2C_{S_n^{2-}} \quad (1)$$

and in the poly(ALA) layer,

$$\overline{C}_{Li^+} = \overline{C}_{TFSI^-} + \overline{C}_{COO^-} + 2\overline{C}_{S_n^{2-}} \quad (2)$$

At equilibrium, the electrochemical potential of each ion in the two phases is equal. For simplicity, the activity coefficient is assumed to be unity in the further derivation. For the Li ion, the

electrochemical potential can be expressed as given in equation (3):

$$\mu^{\circ}_{Li^+} + RT\,ln\,C_{Li^+} + F\Psi = \mu^{\circ}_{Li^+} + RT\,ln\,\overline{C}_{Li^+} + F\overline{\Psi} \tag{3}$$

where μ, Ψ, and F denote the chemical potential, electrical potential (Donnan potential), and Faraday's constant, respectively. Similar relationships can be written for the TSFI and PS anions, as given in equations (4) and (5).

$$\mu^{\circ}_{TFSI^-} + RT\,ln\,C_{TFSI^-} - F\Psi = \mu^{\circ}_{TFSI^-} + RT\,ln\,\overline{C}_{TFSI^-} - F\overline{\Psi} \tag{4}$$

$$\mu^{\circ}_{S_n^{2-}} + RT\,ln\,C_{S_n^{2-}} - 2F\Psi = \mu^{\circ}_{S_n^{2-}} + RT\,ln\,\overline{C}_{S_n^{2-}} - 2F\overline{\Psi} \tag{5}$$

By combining equations (3), (4), and (5), the difference in electric potential can be expressed in terms of the concentration ratios of the two phases as equation (6):

$$\frac{F(\overline{\Psi} - \Psi)}{RT} = ln\frac{C_{Li^+}}{\overline{C}_{Li^+}} = ln\frac{\overline{C}_{TFSI^-}}{C_{TFSI^-}} = ln\left(\frac{\overline{C}_{S_n^{2-}}}{C_{S_n^{2-}}}\right)^{1/2} \tag{6}$$

From equation (6),

$$C_{Li^+}C_{TFSI^-} = \overline{C}_{Li^+}\overline{C}_{TFSI^-} \tag{7}$$

$$C^2_{Li^+}C_{S_n^{2-}} = \overline{C}^2_{Li^+}\overline{C}_{S_n^{2-}} \tag{8}$$

By combining equations (2), (7), and (8), an analytical expression for the PS concentration ratio between the electrolyte phase in the cathode and the poly(ALA) layer can be obtained as equation (9):

$$x^3 + \frac{C_{TFSI^-}}{2C_{S_n^{2-}}}x^2 + \frac{\overline{C}_{COO^-}}{2C_{S_n^{2-}}}x - \frac{C_{Li^+}}{2C_{S_n^{2-}}} = 0$$
$$\sqrt{\frac{\overline{C}_{S_n^{2-}}}{C_{S_n^{2-}}}} = x \tag{9}$$

Equation (9) can be numerically solved using a Newton-Raphson procedure. The PS concentration in the poy(ALA) layer decreases with the increase in the carboxylate concentration in the poly(ALA) layer and with the decrease in the TFSI concentration. Therefore, a higher PS rejection is expected with lower LiTFSI salt concentration in the bulk electrolyte. This calculation indicates that the PS concentration in the poly(ALA) layer could be much lower than that in the cathode electrolyte phase. The other important parameter affecting PS permeation rate is PS diffusion rate through poly(ALA). The electrostatic repulsion between the PS anions and carboxylates of the poly(ALA) and the lowered free volume by the poly(ALA) chains would decrease PS diffusivity.

The above consideration provides conceptual understanding of the driving force for the PS rejection behavior. However, the PS rejection behavior in a real Li–S system is more complex; the PS fluxes originating from concentration gradient across the poly(ALA) layer and migration of PS anions from potential gradient should be considered. Also, the PS concentration at cathode should vary with time. In order to exactly describe the PS rejection process in Li–S batteries, charge and mass balances at non-steady state condition are necessary together with Donnan exclusion theory.

S6. Li ion conduction through the poly(ALA) layer

A film of poly(ALA), synthesized by thermal polymerization was coated on a polyethylene terephthalate (PET) substrate, and then immersed in the reference electrolyte for 12 h to measure the degree of electrolyte absorption. The electrolyte uptake amount was determined by the following equation: Uptake amount (wt%) = $[(W - W_0)/W_0] \times 100$, where W and W_0 are the weights of the poly(ALA) layer after and before electrolyte absorption, respectively. The weight ratio of the electrolyte to the poly(ALA) was 146%, which is comparable to those for polymer electrolytes based on polyvinylidene difluoride (PVdF). The ionic conductivity of the electrolyte-swollen poly(ALA) was determined by measuring the ohmic resistance of the cell with two blocking SUS electrodes and a poly(ALA)-coated polypropylene separator fully equilibrated with the reference electrolyte. The thickness of the poly(ALA) layer was 6 μm. The ohmic resistance was 3.7 Ω cm^2, which corresponds to an ionic conductivity of 2.09×10^{-4} S cm^{-1}. This is quite comparable to that of the reference electrolyte (2.28×10^{-4} S cm^{-1}), indicating that Li ion transport is not significantly retarded by the poly(ALA) layer. In addition to the electrolyte swollen in the poly(ALA) layer, the carboxylate anions attached to the poly(ALA) would contribute to the Li ion transport through the poly(ALA) layer, resulting in the high ionic conductivity.

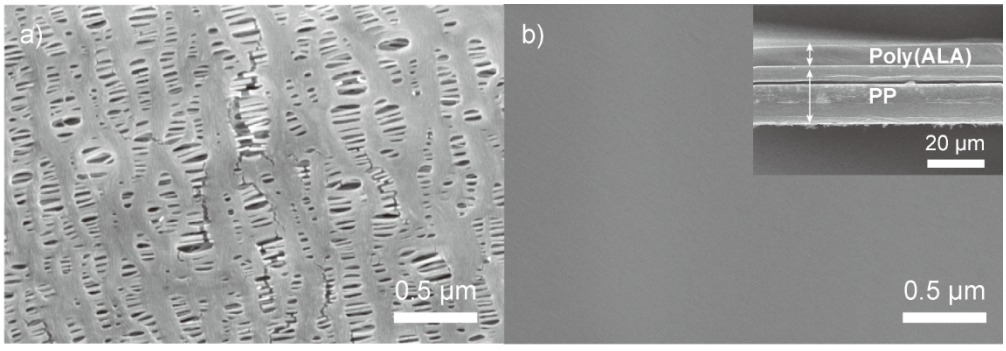

Fig. S6. SEM images of (a) pristine and (b) poly(ALA) coated PP separator for ionic conductivity measurement. Inset of (b) represents the cross-sectional image of the separator.

Supplementary References

1. Yuan, L., Qiu, X., Chen, L. & Zhu, W. New insight into the discharge process of sulfur cathode by electrochemical impedance spectroscopy. *J. Power Sources* **189**, 127-132 (2009)
2. Kolosnitsyn, V.S., Kuzmina, E.V., Karaseva E.V. & Mochalov, S.E. A study of the electrochemical process in lithium–sulphur cells by impedance spectroscopy. *J. Power Sources* **196**, 1478-1482 (2011)
3. Barchasz, C., Lepretre, J.-C., Alloin, F. & Patoux, S. New insights into the limiting parameters of the Li/S rechargeable cell. *J. Power Sources* **199**, 322-330 (2012)
4. Deng, Z., Zhang, Z., Lai, Y., Liu, J., Li, J. & Liu, Y. Electrochemical impedance spectroscopy study of a lithium/sulfur battery:Modeling and analysis of capacity fading. *J. Electrochem. Soc.* **160**, A553-A558 (2013)